



Direct contractility measurement in cardiomyocytes via thin PDMS diaphragm integration with a moving coil actuator: Synergistic maturation through combined topographical and mechanical stimulation

Abdullah^{a,1}, Arunkumar Shanmugasundaram^{a,b,1}, Yun-Jin Jeong^{a,b}, Pooja P. Kanade^a, Jongyun Kim^a, Dong-Weon Lee^{a,b,c,*}

^a School of Mechanical Engineering, Chonnam National University, Gwangju 61186, Republic of Korea

^b Advanced Medical Device Research Center for Cardiovascular Disease, Chonnam National University, Gwangju 61186, Republic of Korea

^c Center for Next-Generation Sensor Research and development, Chonnam National University, Gwangju 61186, Republic of Korea

ARTICLE INFO

Keywords:

PDMS diaphragm
Moving coil actuator
Controlled mechanical stimulation
Enhanced maturation
Direct contractility measurement
Drug screening platform

ABSTRACT

Mechanical stimulation within diaphragm-based cell culture platforms presents a promising strategy to enhance cardiomyocyte maturation. However, most of the proposed techniques have met with limited success due to their inability to directly measure the contractile force of cardiomyocytes. This issue primarily stems from the typically thicker diaphragm structure which is necessary to withstand high strain ranges induced by mechanical stimulation. Herein, we propose a moving coil actuator integrated with a thin polydimethylsiloxane (PDMS) diaphragm for precise mechanical stimulation, cell culture, and drug screening applications. This mechanical stimulation system generates desired mechanical deformation to cultured cardiomyocytes without compromising the integrity of the diaphragm structure. The 10 μm thin diaphragm produces significant displacement from the contractility of cultured cardiomyocytes, which can be directly measured using a laser vibrometer system. Cardiomyocytes cultured on nanogroove PDMS diaphragms with and without stimulation and flat diaphragms with stimulation exhibited 4.25-, 2.81-, 2.39-fold enhancements in contraction force and 1.09-, 1.06-, 1.04-, and 1.32-, 1.17-, 1.16-fold enhancements in sarcomere lengths and Connexin 43 (Cx43) compared to counterparts cultured on flat and nanogroove PDMS diaphragms without stimulation. The practicality of the device as a drug screening platform is demonstrated by examining the drug-induced effects on cardiomyocytes using cardiovascular drugs.

1. Introduction

Cardiovascular diseases are the primary cause of global mortality. As a result, several cardiovascular drugs have been developed to reduce cardiovascular mortality rates [1]. Despite significant progress in drug development, a considerable number of these drugs have been withdrawn from the market due to drug-induced cardiotoxicity [2,3]. A primary reason for this cardiotoxicity is the use of immature cardiomyocytes in in vitro drug screening platforms for cardiotoxicity assessment. These immature cardiomyocytes inadequately replicate the native physiological characteristics of adult cardiomyocytes during drug screening procedures [4–8]. Therefore, there is an imperative need to develop a drug screening platform fortified with a functional tissue

engineering substrate to enhance the maturation, physiology, and metabolic activity of cardiomyocytes.

Over the years, several techniques have been proposed to facilitate the in vitro maturation of cardiomyocytes [9–11]. Among these methodologies, topographical and mechanical stimulations have gained considerable attention due to their ability to replicate in vivo physiological conditions [12–15]. Topographical stimulation, characterized by the application of groove patterns, aligns cardiomyocytes in a specific direction, thereby mimicking the natural alignment and structure of the heart's extracellular matrix and promoting structural maturation [12]. On the other hand, mechanical stimulation, which replicates physiological mechanical cues experienced by the heart, such as cyclic contraction and relaxation, has shown potential in enhancing

* Corresponding author at: School of Mechanical Engineering, Chonnam National University, Gwangju 61186, Republic of Korea.

E-mail address: mems@jnu.ac.kr (D.-W. Lee).

¹ Authors are equally contributed.

cardiomyocyte maturation and contractile properties and in promoting sarcomere organization [15–26].

Incorporating mechanical stimulation into diaphragm or muscular thin film platforms has garnered significant interest, as these platforms mimic in vivo microenvironments found in the extracellular matrix. For instance, Kamotani et al. proposed a platform that integrates piezoelectrically actuated pins with a flexible bottom membrane to foster the maturation of cardiomyocytes [27]. Similarly, Deguchi et al. introduced a piezoelectrically actuated micro stretched platform designed to enhance cardiomyocyte maturation, with an added feature of real-time imaging capability [28]. Nevertheless, the friction between the piezoelectrically actuated pins and the small driving range of piezoelectric actuator limits the practical application of these devices. Moraes et al. proposed a pneumatic actuator-based mechanical stimulation system for cell culture [29]. However, the lubricant used in the pneumatic actuators could potentially contaminate cardiomyocytes during long-term mechanical stimulation. Another system utilizing serially connected pneumatic balloons applies varying strains to each diaphragm via the pressure drop effect [30]. However, controlling the pressure exerted on the diaphragm using this mechanical stimulation system poses significant challenges.

Recently, next-generation cell culture platforms have been proposed that offer controllable strain ranges to cultured cardiomyocytes. For example, Jeong et al. introduced an on-stage bioreactor platform integrated with a nano patterned PDMS diaphragm and mechanical stimulation for live cell stimulation and imaging [10]. While this platform exhibited superior performance compared to other reported mechanical stimulation systems, the proposed system was not suited for measuring the contraction force of the cardiomyocytes. Similarly, Siddique et al. proposed a PDMS diaphragm integrated with mechanical stimulation and investigated the combined impact of topographical and mechanical stimulation on the structural and functional anisotropy of cardiomyocytes [31]. The effects of mechanical stimulation on the contractility and maturation of cardiomyocytes cultured on the PDMS diaphragm were assessed using an inverted microscope through video acquisition and image tracking analysis. In another study, Dou et al. proposed a microdevice platform designed to characterize the effects of varying mechanical strain magnitudes on cultured cardiomyocytes [32]. Cardiomyocyte contractility was investigated using fluorescent beads via traction force microscopy. However, these methodologies had limited success due to their inability to directly measure the contractile force of cardiomyocytes. This limitation mainly arises from the need for a thicker diaphragm structure that can sustain the high strain ranges provided by mechanical stimulation.

To overcome the drawbacks of the current state-of-the-art, two critical issues need to be addressed. The first issue is to reduce the thickness of the cell culture platform, preferably to a few micrometers. The second issue involves developing a mechanical stimulation system capable of generating minuscule pressure to provide the desired

mechanical stimulation to cardiomyocytes. In this work, we have attempted to address these limitations by developing a moving coil actuator integrated with a PDMS diaphragm for precise mechanical stimulation, cell culture, and drug screening applications. The thin 10 μm diaphragm produces significant displacement resulting from the contraction and relaxation of cultured cardiomyocytes, and this can be directly measured using a laser vibrometer. The moving coil actuator-based mechanical stimulation system generates the desired mechanical deformation to the cultured cardiomyocytes without compromising the diaphragm structural integrity. Cardiomyocytes, obtained from the NRVM isolation process, are cultured on the PDMS diaphragm platform both with and without mechanical stimulation. The cardiomyocytes on the platform demonstrate strong adhesion to the substrate and display enhanced maturity due to the synergistic effects of topographical and mechanical stimulation. These mature cardiomyocytes exhibited significantly enhanced responsiveness to cardiovascular drugs such as verapamil and quinidine compared to their immature counterparts (Fig. 1).

2. Materials and methods

2.1. Concept and mechanism of the PDMS diaphragm with an integrated moving coil actuator

The conceptual framework and working mechanism of the proposed moving coil actuator integrated PDMS diaphragm are schematically illustrated in Fig. 2. Fig. 2a depicts the experimental setup, designed for cell culture, maturation enhancement, and investigation of drug-induced cardiotoxicity. This setup comprises a function generator, laser vibrometer, stage-top incubator, and an XYZ motorized stage. A function generator is employed to accurately regulate the mechanical stimulation by supplying voltage based on the coil resistance for optimal performance. An air inlet is utilized to administer mechanical stimulation. The nanogroove-patterned PDMS diaphragm with a laser reflection point is used to analyze cardiomyocyte contractility by measuring diaphragm displacement using a laser vibrometer. The details of the laser vibrometer and its related parameters are provided in the [supplementary information](#). The stage-top incubator is used to control the cell culture environment. The stage-top incubator is used to control the cell culture environment.

Since the top PDMS diaphragm is made of from a 10 μm -thin PDMS film, precise management of the pressure exerted on this diaphragm is paramount. Excessive or inappropriate pressure can compromise the structural integrity of this PDMS layer, making controlled mechanical stimulation a challenging task. Considering the delicate nature of the top PDMS diaphragm, our design strategy incorporated a sturdier bottom PDMS diaphragm. This not only serves as a protective cushion beneath the thin top PDMS membrane but also moderates strain stemming from mechanical stimulations, thus ensuring superior control over the

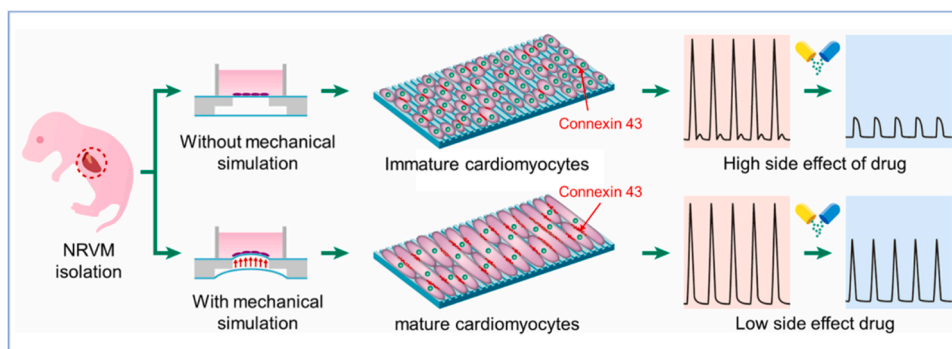


Fig. 1. Diagram depicts NRVM-differentiated cardiomyocytes cultured on a moving coil actuator-integrated PDMS diaphragm with or without mechanical stimulation. Mature cardiomyocytes on this platform, under mechanical stimulation, showed improved response to cardiovascular drugs than immature ones.

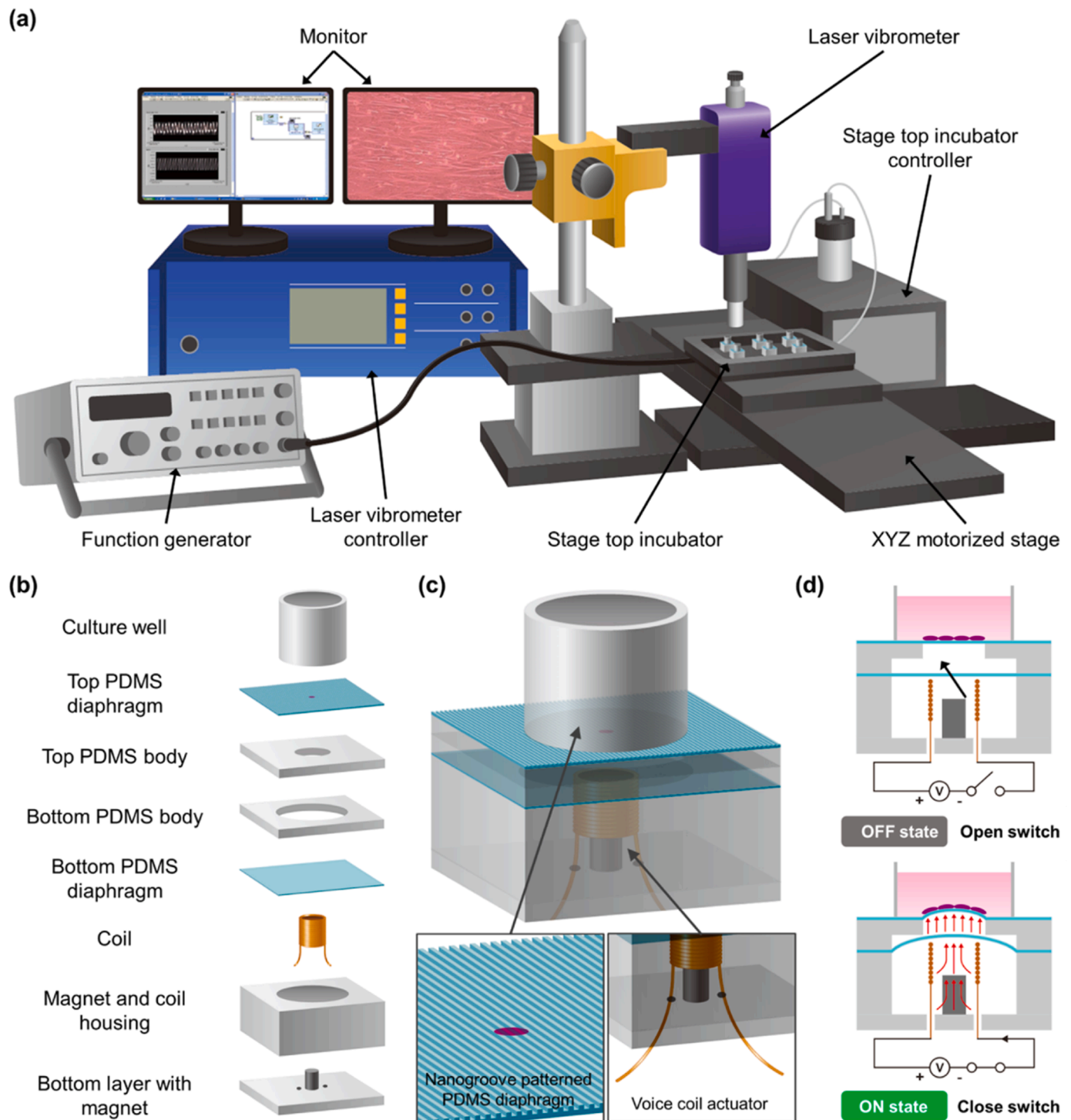


Fig. 2. Concept and operation of the proposed drug screening device. **(a)** Diagram of the setup for cardiomyocyte culture, maturation, and drug testing. **(b)** Assembly and components of the well plate, featuring a PDMS diaphragm and a moving coil actuator. **(c)** Schematic of the moving coil actuator-diaphragm platform. **(d)** Electromagnetic actuator function: (1) off state without current, and (2) on state with current, moving the PDMS diaphragm to stimulate cultured cardiomyocytes.

mechanical stimulation process. The proposed device designed in such a way that the bottom PDMS diaphragm interfaces directly with the mechanical stimulator. In contrast, the top layer senses mechanical stimulation through the air pressure generated by the bottom layer. In this context, the voice coil actuator also known as moving coil actuator plays a pivotal role. A moving coil actuator is a type of electromagnetic actuator that operates based on the principles of Lorentz force. When a current-carrying conductor is placed within a magnetic field, it experiences a force perpendicular to both the current and the magnetic field.

Its precise control and response characteristics are invaluable in ensuring the exact pressure and movement required for the system, especially given the fragility of the thin, soft materials like PDMS. The moving coil actuator's ability is to deliver consistent and accurate mechanical stimuli while safeguarding the delicate structures. Besides, the mechanical stimulation range can be easily controlled by controlling the applied current passing through the coil. Fig. 2b schematically illustrates the proposed device, which comprises a culture well, a 10 μm -thick top PDMS diaphragm, top and bottom PDMS bodies, a coil, coil

housing, and a bottom layer with a magnet. The proposed device encompasses an electromagnetically actuated diaphragm with an attached copper coil, a permanent magnet, a PDMS diaphragm featuring 800 nm nanogroove patterning, and a laser reflection point, as well as a cell culture well (Fig. 2c). Fig. 2d illustrates the working mechanism of the proposed moving coil actuator-based mechanical stimulation system.

2.2. Fabrication of reusable nanogroove patterned PUA mold

In the typical fabrication process, the nanogroove-patterned AZ-GXR-601 photoresist substrate was first produced using a reusable nanogroove-patterned PDMS mold (Fig. S1). First, we fabricated a nanogroove-patterned polyurethane acrylate (PUA) mold using the following steps. A precalculated amount of PUA liquid precursor was poured onto the master silicon mold. Then, a 125 μm -thick polyethylene terephthalate (PET) support film was gently pressed onto the PUA resin. Subsequently, by gently rolling a roller on the surface of the PET film, a uniform PUA film was formed on the silicon mold. This PUA film was then exposed to UV light with an exposure energy of $\sim 20 \text{ mJ cm}^{-2}$ for 10 h. After the UV curing process, the nanogroove-patterned PUA mold, which was attached to the PET, was carefully detached from the master silicon mold (Fig. S1a).

2.3. Fabrication of reusable nanogroove patterned PDMS mold

The PDMS mixture was prepared by mixing a 10:1 ratio of base polymer to curing agent and was then placed in a vacuum desiccator for 30 min to remove air bubbles. This PDMS mixture was subsequently spin-coated onto the PUA mold at 700 RPM for 40 s and degassed in a vacuum desiccator for 10 min (Fig. S1b). A 125 μm -thick PET support film was gently pressed onto the PDMS before the film was cured at 100°C for 1 h using a preheated hot plate. After curing, the nanogroove-patterned PDMS film was gently removed from the PUA mold (Fig. S1c). The thickness of the PDMS layer was successfully controlled by maintaining consistent PDMS viscosity, spin-coating duration, and speed.

2.4. Fabrication of reusable nanogroove patterned AZ-GXR-601 photoresist

A calculated amount of hexamethyldisilane (HDMS) was spin-coated onto a silicon substrate at 4000 RPM for 40 s (Fig. S1d). Subsequently, the HDMS-coated silicon substrate was placed on a smooth level surface, and a calculated amount of AZ-GXR-601 was poured onto the center of the silicon substrate. The fabricated PDMS mold was then gently pressed onto the AZ-GXR-601-coated silicon substrate (Fig. S1e). After that, a weight with a smooth surface was placed on the PDMS mold to ensure uniform force distribution and the formation of AZ-GXR-601 nanogrooves for one hour. This was followed by a soft bake at 110°C for 2 h. Finally, the PDMS mold was detached from the silicon substrate, realizing the nanogroove-patterned AZ-GXR-601 mold (Fig. S1f).

2.5. Properties of the designed moving coil actuator

The designed actuation mechanism, powered by the moving coil actuator, is engineered to induce strains varying from 2% to 10% on the 10 μm thin top PDMS diaphragm. This moving coil actuator consists of a cylindrical coil featuring 150 turns, with dimensions of 7 mm in length and 6 mm in width. The armature of this cylindrical coil is reinforced by craft paper with a thickness of 7 mm and is securely bonded using an adhesive resin boasting high thermal conductivity. The coil wires are meticulously twisted and sheathed with metallic meshes to enhance electromagnetic interference resistance. The coil exhibits a resistance of approximately 4.3Ω , and when placed within a magnetic field, its inductance measures at $114.23 \mu\text{H}$. Detailed properties of the designed moving coil actuator are shown in Table S1. This linear moving coil actuator incorporates a neodymium magnet with dimensions of 3 mm in

diameter and 5 mm in height, situated within the actuator assembly. According to the Lorentz force principle, a force materializes when a current traverses the coil in the presence of a magnetic field. This relationship is concisely expressed by the equation:

$$F = NBIL$$

Where: F represents the Lorentz force, N stands for the number of effective coils turns, B denotes the average magnetic flux density, I symbolize the excitation current through the coil, and L signifies the effective length over which the Lorentz force is generated. For the proposed moving coil actuator, N is valued at 150, L is 16 mm, and B averages at 556 mT. Consequently, with the application of a continuous current ranging from 0.2 to 1 A to the coil, the moving coil actuator produces a consistent displacement between 1300 ± 60 – $2017 \pm 52 \mu\text{m}$. This displacement spectrum aligns with the requisite force to achieve 6–10% strain on the 10 μm -thick upper PDMS diaphragm.

2.6. Fabrication of moving coil actuator integrated nanogroove PDMS diaphragm

A 10 μm -thick PDMS layer was spin-coated onto the AZ-GXR-601 photoresist for 40 s at 6000 RPM, and subsequently cured at 80°C for 2 h using a preheated hot plate. A laser reflection pattern was then imprinted on the PDMS layer using a shadow mask and photolithography techniques. The nanogroove-patterned PDMS layer was attached to a 2 mm-thick PDMS layer to form the diaphragm structure through oxygen plasma treatment (FEMTO SCIENCE, CUTS-MPR). The AZ-GXR-601 photoresist sacrificial layer was subsequently removed using acetone to produce the nanogroove-patterned PDMS diaphragm. The culture ring was bonded to the nanogroove-patterned PDMS diaphragm to form the cell culture platform (Fig. S2a). A FE-SEM image demonstrated the well-defined shape, size, and fidelity of the fabricated nanogroove-patterned PDMS diaphragm (Fig. S2b). A neodymium magnet, 3 mm in diameter and 5 mm in height, was placed inside a moving coil actuator that measured 7 mm in height and 6 mm in diameter and was composed of copper (Fig. S3). The details of the magnet coil housing are schematically illustrated in Fig. S4. The magneto-mechanical components, speaker, and nanogroove PDMS diaphragm were carefully optimized, as discussed in the results and discussion section. When voltage was applied to the moving coil actuator, it and the 20 μm PDMS diaphragm functioned as a speaker. The first component of the top part comprised a 10 μm PDMS diaphragm, which consisted of two PDMS layers: one serving as a buffer layer and the other as a pressure cavity. The second component of the top part included a 10 μm PDMS diaphragm, a PDMS layer with an 8 mm central hole, and a pressure cavity with a 16 mm central hole. The optimized electromagnetically actuated moving coil actuator was attached to the bottom of the PDMS diaphragm, providing mechanical stimulation to the cardiomyocytes cultured on the thin 10 μm diaphragm (Fig. S5a). The dimensions of the fabricated platform, integrated with the electromagnetic actuator, were determined to be 16 mm in height, with the pressure cavity's central hole measuring 16 mm (Fig. S5b).

2.7. Statistical analysis

Statistical analysis was conducted using one-way analysis of variance (ANOVA) followed by Tukey's honest significant difference test in Origin software to assess the statistical significance between three biologically independent samples. The data are presented as the mean \pm standard error of the mean (S.E.M.). Significance levels were designated at $* p < 0.01$. Rise time and decay time were analyzed and corrected using Fridericia's formula (corrected duration = absolute duration/(interspike interval) $^{1/3}$).

3. Results and discussion

3.1. Preliminary characteristics of the moving coil actuator integrated PDMS diaphragm

The optimal design strategy for the platform was essential to achieve the desired diaphragm displacement and adequate mechanical stimulation for cardiomyocytes cultured on the PDMS diaphragm. The optimal parameters for cell culture diaphragm thickness, diameter, and bottom diaphragm thickness were ascertained through a series of experiments and simulations (Fig. 3, S6). The various parts of the platform such as the top and bottom PDMS diaphragm, laser reflecting area, and top and bottom PDMS body is schematically illustrated in Fig. 3a. Firstly, we examined the relationship between the thickness and hole diameter of the top PDMS diaphragm to achieve maximum displacement, as depicted in Figs. S7(a-c). The displacement of the top PDMS diaphragm (thickness of 10 μm and a diameter of 8 mm) in response to various applied currents supplied to the moving coil actuator was examined by varying the bottom PDMS diaphragm thickness within a range of 10–100 μm (Fig. 3b). Voltage was applied using a function generator operating at a frequency of 1 Hz; this was subsequently converted to current based on the measured coil resistance (4.3 Ω). A decrease in PDMS diaphragm thickness led to an increase in PDMS diaphragm displacement as the applied current increased. The maximum and minimum changes in displacement occurred at thicknesses of 10 μm and 100 μm , respectively, yielding corresponding displacements of $190 \pm 3 \mu\text{m}$ and $89 \pm 3.6 \mu\text{m}$ when the generated current reached 1 A. Since the bottom PDMS diaphragm directly interfaces with the voice coil actuator, it is crucial for the bottom diaphragm to be resilient enough to endure the direct mechanical stimulation. By having an identical 10 mm diameter for both diaphragms, they would undergo similar deformations. However, a thicker diaphragm demands greater pressure to achieve the same displacement as its thinner counterpart. The simulations results shown in Fig. S7(d) and (e) demonstrates the external forces requisite for generating a strain of 10% on top PDMS diaphragm of varying bottom PDMS diaphragm thicknesses (10–30 μm). Predictably, the necessary force for a 10% mechanical stimulation rises with an increase in the thickness of the bottom diaphragm. The comprehensive analysis revealed that a 20 μm thickness for the bottom diaphragm increase the sensitivity of the top diaphragm by approximately eight-fold, as opposed to when the actuator directly engages with the top diaphragm. Therefore, 20 μm was selected as the optimized thickness for bottom PDMS diaphragm despite the displacement maximum at 10 μm after careful consideration of both the mechanical and practical constraints.

Fig. 3c shows the displacement of the bottom PDMS diaphragm, which has a thickness of 20 μm , in relation to the varying diameter of the same diaphragm, ranging from 8 to 16 mm, under different applied currents. As the diameter of the diaphragm increased from 8 mm to 16 mm, alongside an increase in the applied current, the displacement of the bottom PDMS diaphragm similarly increased. The maximum displacement recorded was $590 \pm 3.5 \mu\text{m}$ at 1 A, observed in the bottom diaphragm that had a thickness of 20 μm and a diameter of 16 mm. Based on these analyses, we fabricated a platform featuring a top PDMS diaphragm with a thickness of 10 μm and a hole diameter of 8 mm, in combination with a bottom PDMS diaphragm having a thickness of 20 μm and a hole diameter ranging from 8 to 16 mm. Subsequently, we measured the displacement of the top PDMS diaphragm under various applied current levels (Fig. 3d). The displacement of the top PDMS diaphragm increased with the increase in the bottom diaphragm hole diameter from 8 to 16 mm. The top PDMS diaphragm achieved the maximum displacement of $2070 \pm 52 \mu\text{m}$ when the applied current was 1 A.

Based on the preceding analyses, we optimized the design with a top PDMS diaphragm thickness of 10 μm , a hole diameter of 8 mm, a bottom diaphragm thickness of 20 μm , and a hole diameter of 16 mm. This

combination was chosen for further analyses as it yielded the maximum displacement compared to other combinations. As depicted in Fig. 3e and f, we investigated the displacement of the top PDMS diaphragm in relation to various applied currents, both with and without the presence of culture media. At 1 A applied current, the top PDMS diaphragm achieved the maximum displacements of $1650 \pm 67 \mu\text{m}$ and $2070 \pm 52 \mu\text{m}$, in the presence and absence of culture media, respectively. Then, the relationship between the strain values and corresponding to the PDMS diaphragm as a function of applied current was investigated using finite element analysis (FEA) simulations. The displacement and strain values of a PDMS diaphragm with a thickness of 10 μm were examined in relation to a varying hole diameter range of 8 – 16 mm (Fig. S6a). The displacement changes observed when increasing the PDMS diaphragm hole diameter from 8 mm to 16 mm were 0.16, 0.59, 1.22, and 2.02, correlating to strain ranges of 2%, 4%, 6%, and 10%, respectively. These changes were achieved by generating a consistent electromagnetic force of $3.60 \times 10^{-3} \text{ N/A}$ while maintaining a steady 1 A current. The PDMS diaphragm displacement and its corresponding strain variation demonstrated a linear relationship. Maximum displacements and strains were recorded as $2.07 \pm 0.052 \text{ mm}$ and $10 \pm 0.251\%$ without media, and $1.65 \pm 0.067 \text{ mm}$ and $7.97 \pm 0.323\%$ with 1 mL of media, respectively (Fig. S6b).

The strain produced by the moving coil actuator on the PDMS diaphragm was investigated using the finite element method simulation analysis. The Neo-Hookean hyperelastic model was adopted for our simulation. For the PDMS membrane, we specified a Young's modulus of 750 kPa and a Poisson's ratio of 0.48. We implemented a 2-D axisymmetric model, with fixed constraints applied. At one end of the plate, fixed boundary conditions were imposed. A uniformly distributed load of 2.2 kPa was directed to the bottom surface of the top PDMS membrane. Our simulation utilized a tetrahedral mesh, boasting a minimum element size of 3 μm . Mesh is automatically generated by the software. We employed the simulation software, COMSOL Multiphysics (Stockholm, Sweden), targeting the determination of strain on the top surface of the PDMS membrane. For convergence, a criterion was set to a maximum residual of 1000, and each simulation scenario underwent 25 iterations.

Fig. S8(a, b) illustrates the strain contours on the top PDMS membrane in both radial and circumferential directions as derived from the FEA simulation. These contours effectively highlight the spatial distribution of mechanical strains, specifically emphasizing the regions where cardiomyocytes are cultured. The uniformity of strain across this critical area is paramount, underpinning the reliability and reproducibility of our experimental system. The strain profiles of the PDMS diaphragm, subjected to an applied strain of 8%, are shown in Fig. S8(c, d). Analyses of the results indicate a consistent radial strain value that remains invariant with an increasing radial distance from the diaphragm's center. Notably, a negative radial strain is discernible at the fixed peripheral edge of the PDMS diaphragm. In contrast, the circumferential strain decreases with an increasing radial distance, reaching zero precisely at the diaphragm's fixed boundary. Fig. 4d presents a quantitative relationship, mapping the ratio of radial to circumferential strain at 8% applied strain, as a function of the radial distance from the diaphragm's center. This ratio exhibits a gradual increase, peaking at 3.5 mm from the center. Between the central region and a radial distance of 2.5 mm, this ratio varies in the range of 1–1.5. Consequently, for subsequent analyses, cardiomyocytes cultured within a radial span of 2.5 mm from the diaphragm's center were exclusively considered for further analysis.

3.2. Effect of topographical and mechanical stimulation on the cultured cardiomyocytes

We investigated the effect of topographical and mechanical stimulation on the proliferation and maturation of cardiomyocytes cultured on flat and nanogroove PDMS diaphragms, both without and with mechanical stimulation (Fig. 4). Neonatal rat ventricular myocytes (NRVM)

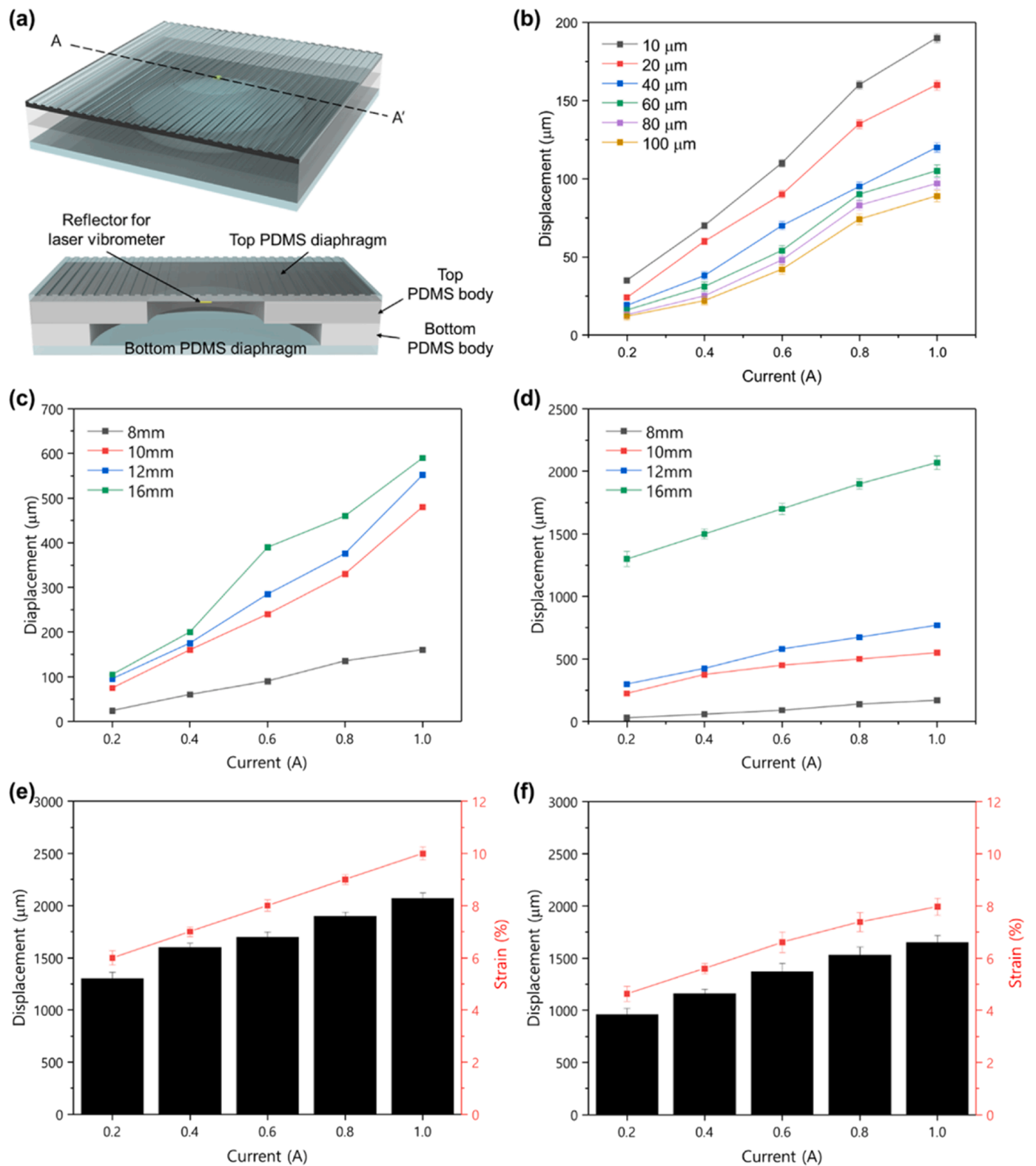


Fig. 3. Design optimization for an integrated moving coil actuator with a PDMS diaphragm. **(a)** PDMS diaphragm components diagram. **(b)** Displacement of a 10 μm thick, 8 mm diameter top diaphragm with respect to variable bottom diaphragm thickness (10–100 μm) under changing currents. **(c)** Displacement of a 20 μm thick bottom diaphragm against its diameter (8–16 mm) at varying currents. **(d)** Displacement response of the top diaphragm to varying bottom diaphragm diameters (8–16 mm) under different currents. **(e, f)** The relationship between top diaphragm displacement and strain at varied currents, without or with culture media, shown in bar plot.

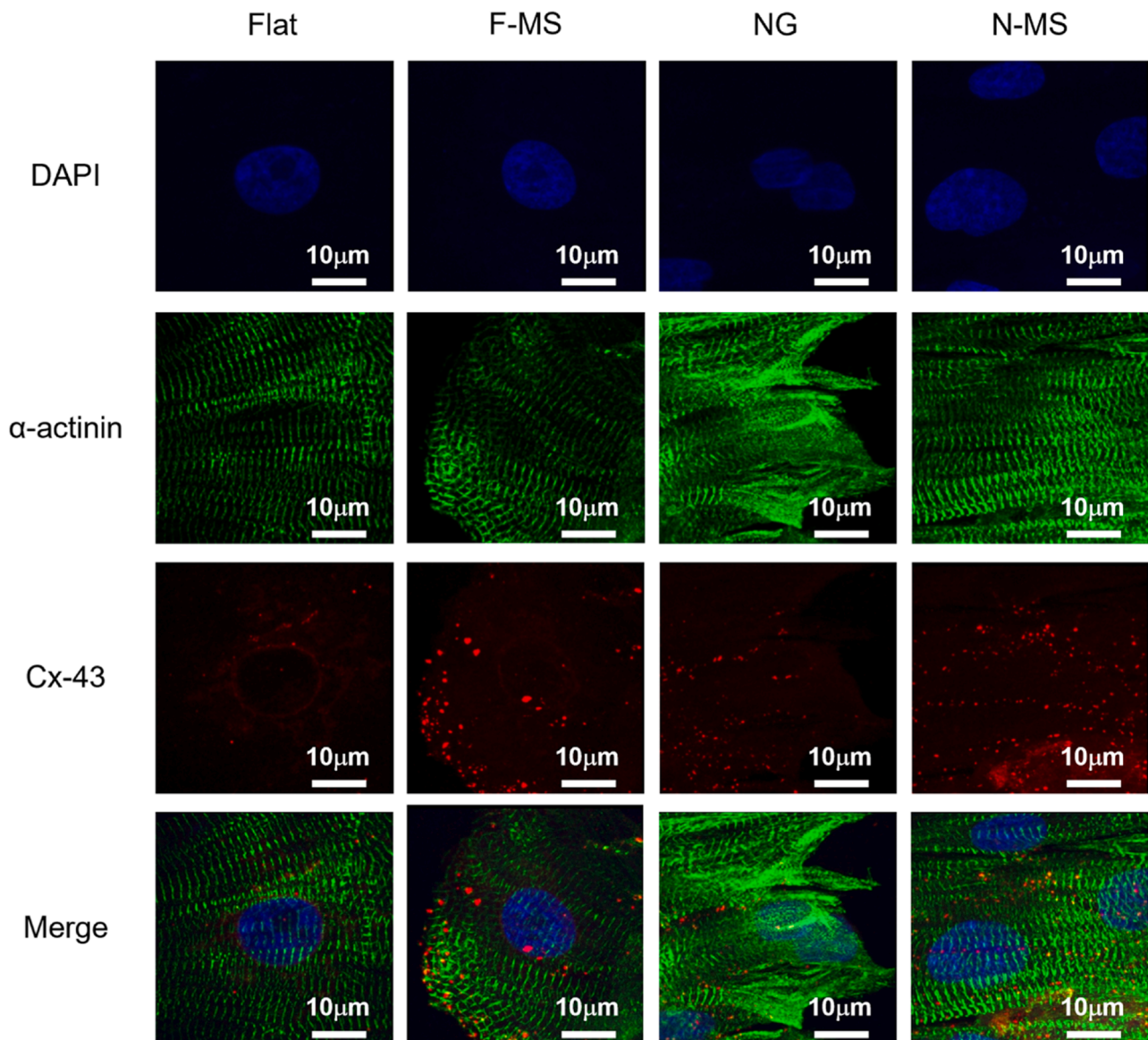


Fig. 4. Immunocytochemical staining analysis of cardiomyocytes cultured on both flat and nanogroove PDMS diaphragms, in the absence and presence of 8% strain mechanical stimulation at a frequency of 1 Hz, on culture day 9. F-MS, NG and N-MS represent flat with mechanical stimulation, nanogrooves, and nanogrooves with mechanical stimulation respectively.

were isolated from the hearts of one-day-old Sprague-Dawley rats. The detailed NRVM isolation process is provided in the [supplementary information](#). All animal experiments were conducted in accordance with the principles of laboratory animal care, relevant national regulations, and received approval from the Animal Ethics Committee at Chonnam National University (license number: CNU IACUC-YB-2023-48). Upon cell culture on the diaphragm as a substrate, the cardiomyocytes started to adhere and grow on the substrate. By the day 3 after cell culture, a monolayer cardiac tissue was formed on the diaphragm. The cells in the cardiac tissue contract and relax spontaneously and synchronously, thereby generating a collective contraction force that resulted in the displacement of the diaphragm. The cardiomyocytes were cultured on both flat and nanogroove PDMS diaphragms with and without mechanical stimulation for a period of 9 days. The displacement of the PDMS diaphragm, due to the contraction and relaxation of cardiomyocytes cultured on both flat and nanogroove PDMS diaphragms, was studied under both the absence and presence of 8% strain mechanical stimulation at a frequency of 1 Hz, from culture day 3–9. Mechanical stimulation was given to the cardiomyocytes continuously from

culture day 3 to day 9, except the duration when the displacement of the diaphragm was measured optically to assess the cardiac contraction force.

The immunocytochemical (ICC) staining analyses on cardiomyocytes cultured on both flat and nanogroove PDMS diaphragms, with and without the application of 8% strain mechanical stimulation at a frequency of 1 Hz, on culture day 9, were investigated. The detailed ICC staining experimental procedure is described in the [supplementary information](#). ICC staining micrographs of cardiomyocytes cultivated on both flat and nanogroove PDMS diaphragms, with and without mechanical stimulation, are shown in [Fig. 4](#). The staining images were analyzed by measuring fluorescence intensity using Image J software. Comparative analysis of these micrographs indicates that the cardiomyocytes grown on nanogroove PDMS diaphragms with mechanical stimulation exhibit more pronounced organization in terms of sarcomere length and Cx43 distribution. This contrasts with cardiomyocytes cultured on flat PDMS diaphragms and nanogroove PDMS diaphragms without mechanical stimulation, where the organization of sarcomere length and Cx43 is less distinct.

The cardiomyocytes cultured on the PDMS diaphragm started producing significant displacement from day 3 of cultivation, coinciding with the onset of synchronized beating. The real-time traces of the PDMS diaphragm displacement caused by the contraction force of the cardiomyocytes are shown in Fig. 5a. The displacement of the PDMS diaphragm increased with the culture day, reaching a maximum on day 9 before declining with further increasing of the culture period, in all PDMS diaphragms, regardless of topographical and mechanical stimulation. However, cardiomyocytes cultured on the nanogroove PDMS diaphragm with mechanical stimulation produced a maximum displacement of $33.6 \pm 5 \mu\text{m}$, compared to the flat PDMS diaphragm ($7.9 \pm 0.5 \mu\text{m}$) and the nanogroove PDMS diaphragm without mechanical stimulation ($22.1 \pm 1.5 \mu\text{m}$). This signifies that the cardiomyocytes cultured on the nanogroove PDMS diaphragm with mechanical stimulation exhibited the highest relative contraction force compared to their counterparts (Fig. 5b). The beat rate of cardiomyocytes cultured on both flat and nanogroove PDMS diaphragms, with or without mechanical stimulation, decreased as the culture day increased (Fig. 5c). The beat rate of the cardiomyocytes cultured on both flat and nanogroove PDMS diaphragms, without and with mechanical stimulation on day 9 were found to be 0.6 ± 0.3 , 0.7 ± 0.2 , and 1 ± 0.1 Hz, respectively. The higher displacement and beat rate observed in the nanogroove PDMS diaphragm with mechanical stimulation suggests improved maturation of the cultured cardiomyocytes.

The sarcomere lengths of cardiomyocytes cultured on flat, nanogroove, and mechanically stimulated PDMS diaphragms under 8% strain were found to be $\sim 1.81 \pm 0.02 \mu\text{m}$, $1.92 \pm 0.03 \mu\text{m}$, and $1.97 \pm 0.03 \mu\text{m}$, respectively (Fig. 5d). The increase in sarcomere length in cardiomyocytes cultured on mechanically stimulated nanogroove PDMS diaphragms can be attributed to the synergistic effects of topographical and mechanical stimulation. Cardiomyocytes demonstrate enhanced sensitivity to their surroundings when cultured on nanogroove surfaces, which facilitate the suppression of the local microenvironment of the cardiomyocytes [33]. Focal adhesion kinases are crucial for cellular responses to mechanical stimulation. During mechanical deformation, mechanical cues from the extracellular environment are potentially transduced via the focal adhesion complex, initiating a signaling cascade that propagates to Z discs for the mechanical coordination of cultured cardiomyocytes, thereby improving sarcomere length [34]. The Cx43 intensities for cardiomyocytes cultured on flat, nanogroove, and mechanically stimulated PDMS diaphragms under 8% strain were approximately 1 ± 0.01 , 1.17 ± 0.02 , and 1.32 ± 0.01 , respectively (Fig. 5e). The increased Cx43 expression in cardiomyocytes exposed to both topographical and mechanical stimuli may result from enhanced electrical conduction across the nanogroove surface and the formation of more functional gap junctions due to external mechanical stimulation [35–37].

3.3. Drug toxicity screening

The practical feasibility of the proposed device as a drug screening platform was demonstrated by analyzing the adverse effects induced by cardiovascular drugs on cardiomyocytes. Specifically, we examined the effect of verapamil and quinidine, two commonly used cardiac drugs, on cardiomyocytes cultured on both flat and nanogroove PDMS diaphragms, with and without mechanical stimulation. To assess the adverse effects of these drugs on cardiomyocytes, we prepared varying concentrations of verapamil and quinidine by diluting the drugs in ethanol and dimethyl sulfoxide (DMSO) respectively, limiting the quantity of ethanol and DMSO to 0.1% of culture media volume. The contractility of the cardiomyocytes was assessed by measuring their relative contraction force before and after the drug treatment. Given that these drugs target different ion channels, their effects on the relative contraction force and overall contractility such as beat rate, rise time, and decay time of the cardiomyocytes were also analyzed.

Firstly, we investigated the adverse effects of verapamil on

cardiomyocytes cultured on both flat and nanogroove PDMS diaphragms, with and without mechanical stimulation. Verapamil, a prevalent L-type calcium channel blocker, is typically employed in the treatment of hypertension, angina, and specific types of arrhythmias [38,39]. Its mechanism of action involves impeding L-type calcium channels, which can attenuate the contractility of cardiomyocytes, resulting in diminished contraction force and a prolonged duration [40, 41]. We administered a range of verapamil concentrations (from 10 nM to 50 μM) to cardiomyocytes cultured on both flat and nanogroove PDMS diaphragms, both with and without mechanical stimulation. We subsequently measured the contractility of the cardiomyocytes as a function of the varying verapamil concentrations (Fig. 6). Real-time traces of cardiomyocyte contractility at different verapamil concentrations are shown in Fig. 6a. Displacements of the flat and nanogroove PDMS diaphragms without and with mechanical stimulation were found to be 10.58 ± 0.58 , 26.8 ± 1.36 , and $38.35 \pm 2.37 \mu\text{m}$, respectively. The displacement of the PDMS diaphragm decreased with an increasing concentration of verapamil, indicating a reduction in the contraction force of the cardiomyocytes as verapamil concentration increased. Post-treatment of cardiomyocytes with 10 μM of verapamil resulted in a decrease in displacement of the flat, nanogroove, and mechanically stimulated cell-cultured diaphragms to 0.44 ± 0.33 , 5.74 ± 1.07 , and $12.97 \pm 0.95 \mu\text{m}$, respectively (Fig. 6b). The beat rate of the cardiomyocytes cultured on the flat and nanogroove PDMS diaphragms, both without and with mechanical stimulation, decreased 4.25, 2.57, and 1.92 times compared to the control group. This observation suggests that verapamil not only decreases the contraction force of cardiomyocytes but also reduces their beat rate (Fig. 6c).

The rise and decay times of cardiomyocytes cultured on both flat and nanogroove PDMS diaphragms, with or without mechanical stimulation, at different concentrations of verapamil are shown in Fig. 6(d, e). Up to a concentration of 200 nM verapamil, the rise time for cardiomyocytes across all culture platforms remained relatively unchanged. However, further increases in the concentration of verapamil led to an increase in the rise time. Specifically, the rise time for cardiomyocytes treated with 10 μM of verapamil increased by factors of 1.97, 1.82, 1.72, and 1.43 compared to their respective control states. Similarly, the decay time of the cardiomyocytes increased following treatment with verapamil concentrations beyond 200 nM. The decay time for cardiomyocytes treated with 10 μM of verapamil increased by factors of 1.77, 1.63, 1.54, and 1.24 compared to their respective control states. The normalized contraction force and beat rate of the cardiomyocytes cultured on both flat and nanogroove PDMS diaphragms, with or without mechanical stimulation, exhibited an exponential decrease with increasing verapamil concentrations. The observed trends adhered to the Hill's function with IC_{50} values of 856 nM, 1.14 μM , 1.52 μM , and 3.03 μM for contraction force, and 90.4, 958.9 nM, 100.4, and 248.1 nM for beat rate, respectively (Fig. 6f, g).

The adverse effects of quinidine, a Class 1a channel blocker recognized for its sodium channel inhibition capabilities, on cardiomyocytes cultured on flat and nanogroove PDMS diaphragms, under conditions with and without mechanical stimulation were investigated (Fig. 7) [42, 43]. Real-time traces for the cardiomyocytes, cultured on these platforms and subjected to different quinidine concentrations from 10 nM to 50 μM (Fig. 7a). It was observed that the relative contraction force of the cardiomyocytes was inversely correlated to the increasing concentrations of quinidine [44,45]. The displacement of the diaphragms caused by the contraction and relaxation of the cardiomyocytes cultured on flat and nanogroove PDMS diaphragms, both with and without mechanical stimulation were approximately 9.83 ± 0.35 – 7.66 ± 0.32 and 22.78 ± 0.75 – 19.59 ± 0.42 and 47.65 ± 1.52 – 43.83 ± 1.14 for concentrations of quinidine ranging from the control group to 50 μM , respectively (Fig. 7b). Moreover, noticeable changes were observed in both the contractile force and the beat rate of cardiomyocytes on flat and nanogroove PDMS diaphragms, regardless of mechanical stimulation, across the entire range of tested quinidine concentrations. Specifically, after

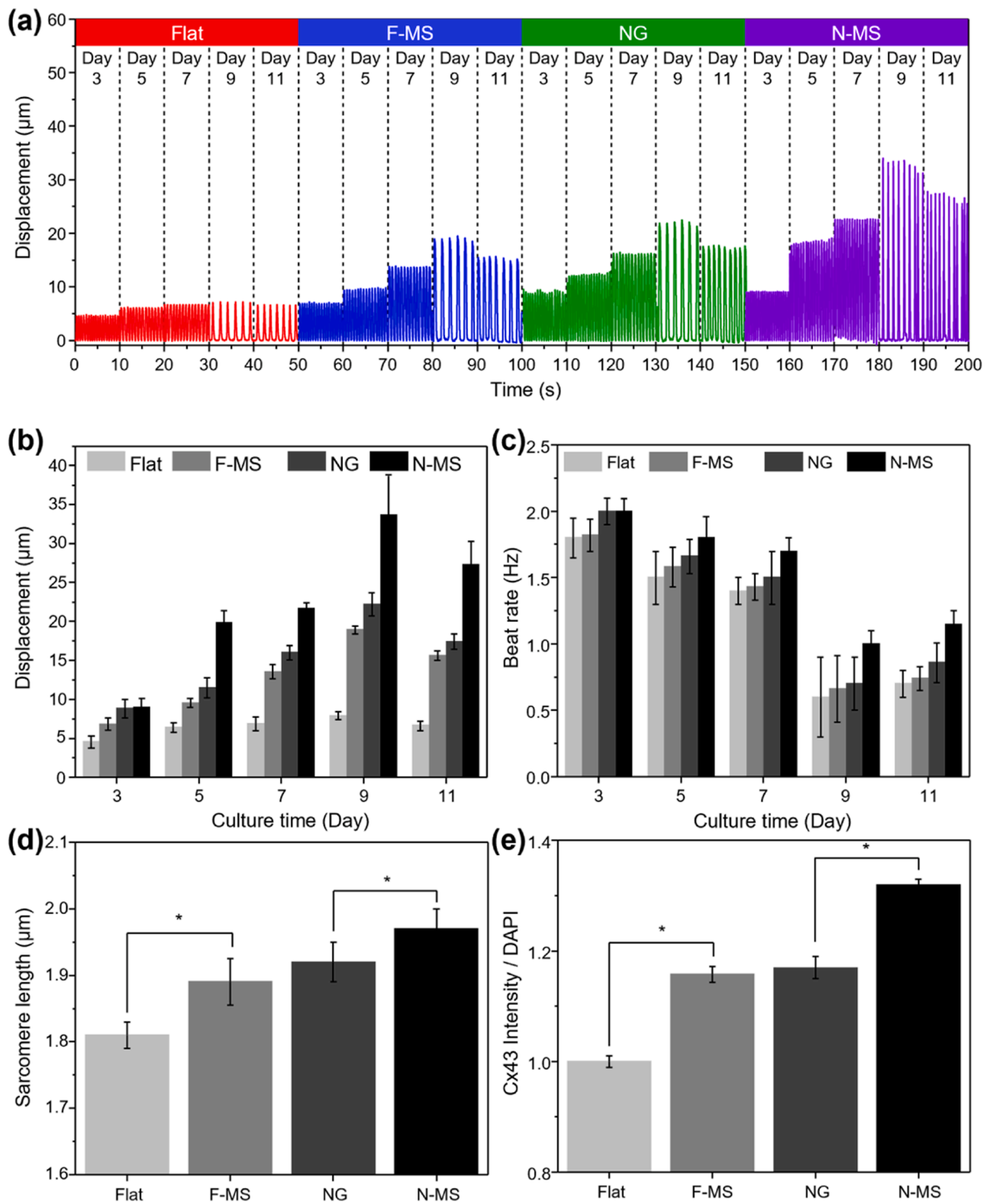


Fig. 5. Synergetic influence of topography and mechanical cues on cardiomyocyte contraction, rhythm, and maturation. **(a)** Real-time traces of cardiac contraction on four types of PDMS diaphragms – flat, F-MS, NG and N-MS. Bar plots of **(b)** displacement and **(c)** beat rates from cells cultured on the different types of diaphragms. **(d, e)** depict sarcomere length and Cx43 expression in cells on the four types of diaphragms, with/without mechanical cues. F-MS, NG and N-MS represent flat with mechanical stimulation, nanogrooves, and nanogrooves with mechanical stimulation respectively.

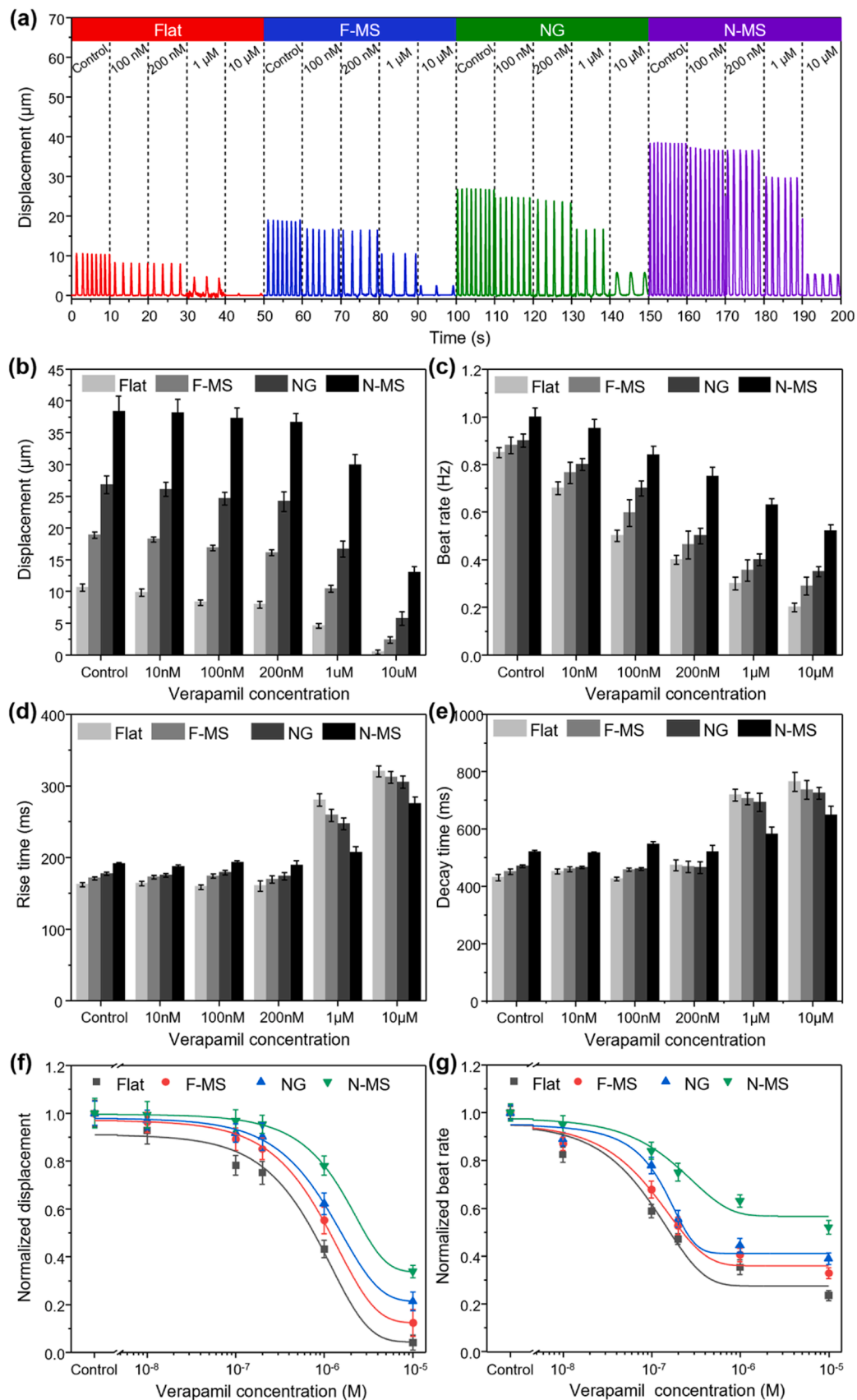


Fig. 6. Effect of verapamil on cardiomyocyte contractility. **(a)** Real-time contractility traces of cardiomyocytes on the four types of PDMS diaphragms – flat, F-MS, NG and N-MS – at various verapamil concentrations. **(b)** Relative contraction force and **(c)** beat rate under different verapamil concentrations. **(d, e)** Rise/decay time at different verapamil concentrations. **(f, g)** Dose-response curve for verapamil showing **(f)** normalized contraction force and **(g)** beat rate. F-MS, NG and N-MS represent flat with mechanical stimulation, nanogrooves, and nanogrooves with mechanical stimulation respectively.

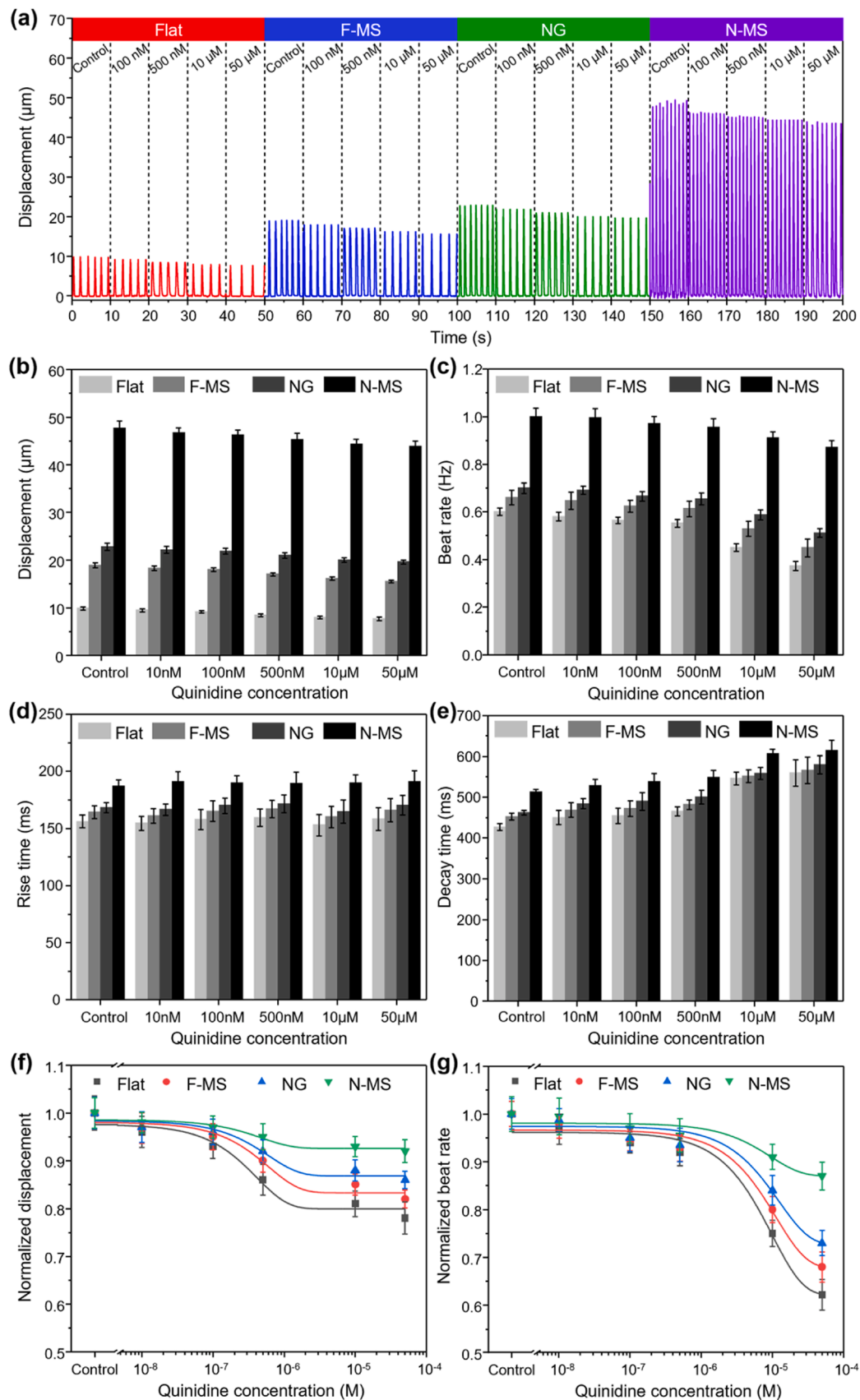


Fig. 7. Effect of quinidine on cardiomyocyte contractility. **(a)** Real-time contractility traces of cardiomyocytes on the four types of PDMS diaphragms – flat, F-MS, NG and N-MS – at various quinidine concentrations. **(b)** Relative contraction force and **(c)** beat rate under different quinidine concentrations. **(d, e)** Rise/decay time at different quinidine concentrations. **(f, g)** Dose-response curve for quinidine showing **(f)** normalized contraction force and **(g)** beat rate. F-MS, NG and N-MS represent flat with mechanical stimulation, nanogrooves, and nanogrooves with mechanical stimulation respectively.

exposure to a quinidine concentration of 50 μM , the beat rates for cardiomyocytes on flat, nanogroove, and mechanically stimulated PDMS diaphragms were determined to be approximately 0.37 ± 0.019 Hz, 0.51 ± 0.018 Hz, and 0.87 ± 0.029 Hz, respectively (Fig. 7c). The rise time of the cardiomyocytes cultured on the aforementioned platforms in the absence and presence of mechanical stimulation was found to be approximately 156 ± 5.6 ms, 168 ± 4.2 ms, and 187 ± 5.4 ms, respectively (Fig. 7d). Subsequent treatment with 50 μM quinidine did not cause a significant change in the rise time of the cardiomyocytes, compared to their respective control states. Contrarily, an increase in the decay time of cardiomyocytes was observed as the quinidine concentration increased. Specifically, when treated with 50 μM quinidine, the decay time of the cardiomyocytes cultured on flat and nanogroove PDMS diaphragm without and with mechanical stimulation was increased to 1.31-fold, 1.25-fold, and 1.19-fold relative to their control states (Fig. 7e). Additionally, a pronounced negative inotropic effect, exhibited as a decreased relative contraction force and beat rate, was associated with increasing quinidine concentrations. The IC_{50} values, calculated from the inotropic effect of the relative contraction force of cardiomyocytes cultured on flat and nanogroove PDMS diaphragms without and with mechanical stimulation, were approximately 198, 221, 256, and 307 nM respectively. Simultaneously, the IC_{50} values derived from the chronotropic effect on the cardiomyocytes were approximately 5.78, 6.42, 8.08 and 9.23 μM respectively. (Fig. 7f, g). In conclusion, both the verapamil and quinidine investigations emphasize the superior drug response of cardiomyocytes cultured on the nanogroove PDMS diaphragm with mechanical stimulation, compared to their counterparts on the flat and nanogroove PDMS diaphragm without mechanical stimulation. Notably, cardiomyocytes on the nanogroove PDMS diaphragm with mechanical stimulation exhibited significantly higher IC_{50} values in both drugs screening studies, indicating a more potent drug dose response owing to superior cell maturation compared to their counterparts.

4. Conclusion

Mechanical stimulation of cultured cardiomyocytes plays a pivotal role in regulating both cellular proliferation and differentiation. The research presented herein centers on the development of a novel moving coil actuator-based mechanical stimulation system, seamlessly integrated with a PDMS diaphragm. This innovative system has been tailored for cell culture, maturation enhancement, and drug screening applications. Our endeavors have successfully overcome the limitations associated with the current state-of-the-art techniques by enabling direct measurement of the contractile force of cardiomyocytes using a laser vibrometer. The personalized moving coil actuator system, a foundation of this research, reliably delivers targeted mechanical stimulation to the cardiomyocytes cultured on the PDMS diaphragm, while preserving the integrity of the delicate diaphragm structure. We further applied the proposed device to mechanically stimulate cardiomyocytes at strain magnitudes of 8%. Our experimental results reveal that both contractility and maturation characteristics of cardiomyocytes are significantly enhanced under mechanical stimulation as compared to cardiomyocytes cultured on flat and nanogroove PDMS surfaces in the absence of mechanical stimulation. Substantial improvements were observed in overall cell alignment, sarcomere length, and Cx43 expression, concomitant with the increase in cardiomyocyte contraction force and contractility. These findings emphasize the critical role of mechanical strain magnitude when establishing in vitro cardiac models, thus ensuring the cellular phenotype closely mirrors that of an adult cardiomyocyte. This enhancement in model accuracy and fidelity greatly improves the applicability of our findings and paves the way for potential clinical translation.

CRedit authorship contribution statement

Abdullah Basham: Conceptualization, Investigation, Validation, Formal analysis, Data curation, Visualization, Writing – original draft. **Arunkumar Shanmugasundaram:** Investigation, Validation, Formal analysis, Writing – original draft, Writing – review & editing. **Yun-Jin Jeong:** Investigation, Validation, Formal analysis, Data curation, Visualization. **Pooja P Kanade:** Investigation, Validation, Formal analysis, Data curation, Visualization. **Jong Yun Kim:** Participated in cardiomyocytes experiments. **Dong-Weon Lee:** Supervision, Funding acquisition, Conceptualization, Writing – review & editing.

Declaration of Competing Interest

The authors declare that they have no known competing for financial interests or personal relationships that could have appeared to influence the work reported in this paper.

Data Availability

Data will be made available on request.

Acknowledgements

This study was supported by a National Research Foundation of Korea (NRF) grant funded by the Korean Government (MSIT) (No. 2020R1A5A8018367 and RS-2022-00165505).

Appendix A. Supporting information

Supplementary data associated with this article can be found in the online version at doi:10.1016/j.snb.2023.134992.

References

- [1] C. Cecilia, L. Wang, C.N. Hess, W.R. Hiatt, A.B. Goldfine, Clinical update: cardiovascular disease in diabetes mellitus 133 (2016) 2459–2502, <https://doi.org/10.1161/CIRCULATIONAHA.116.022194>.
- [2] A. Agarwal, J.A. Goss, A. Cho, M.L. McCain, K.K. Parker, Microfluidic heart on a chip for higher throughput pharmacological studies, *Lab Chip* 13 (2013) 3599–3608, <https://doi.org/10.1039/C3LC50350J>.
- [3] B. Cannon, Cardiovascular disease: biochemistry to behaviour, *Nature* 493 (2013) S2–S3, <https://doi.org/10.1038/493S2a>.
- [4] E. Karbassi, A. Fenix, S. Marchiano, N. Muraoka, K. Nakamura, X. Yang, C. E. Murry, Cardiomyocyte maturation: advances in knowledge and implications for regenerative medicine, *Nat. Rev. Cardiol.* 17 (2020) 341–359, <https://doi.org/10.1038/s41569-019-0331-x>.
- [5] Liu, et al., Human embryonic stem cell-derived cardiomyocytes restore function in infarcted hearts of non-human primates, *Nat. Biotechnol.* 36 (2018) 597–605, <https://doi.org/10.1038/nbt.4162>.
- [6] A. Sizarov, J. Ya, B.A. d Boer, W.H. Lamers, V.M. Christoffels, A.F.M. Moorman, Formation of the building plan of the human heart, *Circulation* 123 (2011) 1125–1135, <https://doi.org/10.1161/CIRCULATIONAHA.110.980607>.
- [7] O. Hudlicka, M.D. Brown, Postnatal growth of the heart and its blood vessels, *J. Vasc. Res.* 33 (1996) 266–287, <https://doi.org/10.1159/000159155>.
- [8] M. Mollova, K. Bersell, S. Walsh, J. Savla, L.T. Das, S.-Y. Park, L.E. Silberstein, C.G. D. Remedios, D. Graham, S. Colan, B. Kühn, Cardiomyocyte proliferation contributes to heart growth in young humans, *Proc. Natl. Acad. Sci.* 110 (2013) 1446–1451.
- [9] D.-S. Kim, Y.-J. Jeong, A. Shanmugasundaram, N.-E. Oyonbaatar, J. Park, E.-S. Kim, B.-K. Lee, D.-W. Lee, 64 PL/PDMS hybrid cantilever arrays with an integrated strain sensor for a high-throughput drug toxicity screening application, *Biosens. Bioelectron.* 190 (2021), 113380, <https://doi.org/10.1016/j.bios.2021.113380>.
- [10] Y.-J. Jeong, D.-S. Kim, J.Y. Kim, N.-E. Oyonbaatar, A. Shanmugasundaram, E.-S. Kim, D.-W. Lee, On-stage bioreactor platform integrated with nano-patterned and gold-coated PDMS diaphragm for live cell stimulation and imaging, *Mater. Sci. Eng. C* 118 (2021), 111355, <https://doi.org/10.1016/j.msec.2020.111355>.
- [11] N.-E. Oyonbaatar, A. Shanmugasundaram, Y.-J. Jeong, B.-K. Lee, E.-S. Kim, D.-W. Lee, Micro-patterned SU-8 cantilever integrated with metal electrode for enhanced electromechanical stimulation of cardiac cells, *Colloids Surf. B: Biointerfaces* 186 (2020), 110682, <https://doi.org/10.1016/j.colsurfb.2019.110682>.
- [12] D. Carson, M. Hnilova, X. Yang, C.L. Nemeth, J.H. Tsui, A.S.T. Smith, A. Jiao, M. Regnier, C.E. Murry, C. Tamerler, D.-H. Kim, Nanotopography-induced

- structural anisotropy and sarcomere development in human cardiomyocytes derived from induced pluripotent stem cells, *ACS Appl. Mater. Interfaces* 8 (2016) 21923–21932, <https://doi.org/10.1021/acsami.5b11671>.
- [13] J. Wang, A. Chen, D.K. Lieu, I. Karakikes, G. Chen, W. Keung, C.W. Chan, R. J. Hajjar, K.D. Costa, M. Khine, R.A. Li, Effect of engineered anisotropy on the susceptibility of human pluripotent stem cell-derived ventricular cardiomyocytes to arrhythmias, *Biomaterials* 34 (2013) 8878–8886, <https://doi.org/10.1016/j.biomaterials.2013.07.039>.
 - [14] K.A. Diehl, J.D. Foley, P.F. Nealey, C.J. Murphy, Nanoscale topography modulates corneal epithelial cell migration, *J. Biomed. Mater. Res., Part A* 75 (2005) 603–611, <https://doi.org/10.1002/jbm.a.30467>.
 - [15] S.A. Biela, Y. Su, J.P. Spatz, R. Kemkemmer, Different sensitivity of human endothelial cells, smooth muscle cells and fibroblasts to topography in the nano-micro range, *Acta Biomater.* 5 (2009) 2460–2466, <https://doi.org/10.1016/j.actbio.2009.04.003>.
 - [16] R.R. Besser, M. Ishahak, V. Mayo, D. Carbonero, I. Claire, A. Agarwal, Engineered microenvironments for maturation of stem cell derived cardiac myocytes, *Theranostics* 8 (2018) 124–140, <https://doi.org/10.7150/thno.19441>.
 - [17] N.T. Feric, M. Radisic, Maturing human pluripotent stem cell-derived cardiomyocytes in human engineered cardiac tissues, *Adv. Drug Deliv. Rev.* 96 (2016) 110–134.
 - [18] I. Nitsan, S. Drori, Y.E. Lewis, S. Cohen, S. Tzliil, Mechanical communication in cardiac cell synchronized beating, *Nat. Phys.* 12 (2016) 472–477, <https://doi.org/10.1038/nphys3619>.
 - [19] X. Tang, P. Bajaj, R. Bashir, T.A. Saif, How far cardiac cells can see each other mechanically, *Soft Matter* 7 (2011) 6151–6158, <https://doi.org/10.1039/COSM01453B>.
 - [20] I. Zhuang, K.A. Yamada, J.E. Saffitz, A.G. Kléber, Pulsatile stretch remodels cell-to-cell communication in cultured myocytes, *Circ. Res.* 87 (2000) 316–322, <https://doi.org/10.1161/01.RES.87.4.316>.
 - [21] V.Y. Sidorov, P.C. Samson, T.N. Sidorova, J.M. Davidson, C.C. Lim, J.P. Wikswo, I-Wire Heart-on-a-Chip I: Three-dimensional cardiac tissue constructs for physiology and pharmacology, *Acta Biomater.* 48 (2017) 68–78, <https://doi.org/10.1016/j.actbio.2016.11.009>.
 - [22] M. Shachar, N. Benishti, S. Cohen, Effects of mechanical stimulation induced by compression and medium perfusion on cardiac tissue engineering, *Biotechnol. Prog.* 28 (2012) 1551–1559, <https://doi.org/10.1002/btpr.1633>.
 - [23] A. Marsano, C. Conficconi, M. Lemme, P. Occhetta, E. Gaudiello, E. Votta, G. Cerino, A. Redaelli, M. Rasponi, Beating heart on a chip: a novel microfluidic platform to generate functional 3D cardiac microtissues, *Lab Chip* 16 (2016) 599–610, <https://doi.org/10.1039/c5lc01356a>. PMID: 26758922.
 - [24] M. Luv, B. André, T. Horvath, A. Nosko, D. Manikowski, D. Hilfiker-Kleiner, A. Haverich, A. Hilfiker, In vitro maturation of large-scale cardiac patches based on a perfusable starter matrix by cyclic mechanical stimulation, *Acta Biomater.* 30 (2016) 177–187, <https://doi.org/10.1016/j.actbio.2015.11.006>.
 - [25] S. Dhein, A. Schreiber, S. Steinbach, D. Apel, A. Salameh, F. Schlegel, M. Kostelka, P.L.M. Dohmen, F.W. Mohr, Mechanical control of cell biology. Effects of cyclic mechanical stretch on cardiomyocyte, *Prog. Biophys. Mol. Biol.* 115 (2014) 93–102, <https://doi.org/10.1016/j.pbiomolbio.2014.06.006>.
 - [26] Q. Wang, H. Huang, Y. Niu, X. Zhang, P. Jiang, K.E. Swindle-Reilly, Y. Zhao, Microscale cell stretcher to generate spatially uniform equi-biaxial strain using an elastomeric membrane with a contoured thickness profile, *Sens. Actuators B Chem.* 273 (2018) 1600–1609, <https://doi.org/10.1016/j.snb.2018.07.051>.
 - [27] Y. Kamotani, T. Bersano-Begey, N. Kato, Y.-C. Tung, D. Huh, J.W. Song, S. Takayama, Individually programmable cell stretching microwell arrays actuated by a Braille display, *Biomaterials* 29 (2008) 2646–2655, <https://doi.org/10.1016/j.biomaterials.2008.02.019>.
 - [28] S. Deguchi, S. Kudo, T.S. Matsui, W. Huang, M. Sato, Piezoelectric actuator-based cell microstretch device with real-time imaging capability, *AIP Adv.* 5 (2015), 067110, <https://doi.org/10.1063/1.4922220>.
 - [29] C. Moraes, J.H. Chen, Y. Sun, C.A. Simmons, Microfabricated arrays for high-throughput screening of cellular response to cyclic substrate deformation, *Lab a Chip* 10 (2010) 227–234, <https://doi.org/10.1039/B914460A>.
 - [30] K. Shimizu, A. Shunori, K. Morimoto, M. Hashida, S. Konishi, Development of a biochip with serially connected pneumatic balloons for cell-stretching culture, *Sens. Actuators B Chem.* 156 (2011) 486–493, <https://doi.org/10.1016/j.snb.2011.04.048>.
 - [31] A.-B. Siddique, A. Shanmugasundaram, J.Y. Kim, A. Roshanzadeh, E.-S. Kim, B.-K. Lee, D.-W. Lee, The effect of topographical and mechanical stimulation on the structural and functional anisotropy of cardiomyocytes grown on a circular PDMS diaphragm, *Biosens. Bioelectron.* 204 (2022), 114017, <https://doi.org/10.1016/j.bios.2022.114017>.
 - [32] W. Dou, L. Wang, M. Malhi, H. Liu, Q. Zhao, J. Plakhotnik, Z. Xu, Z. Huang, C. A. Simmons, J.T. Maynes, Y. Sun, A microdevice platform for characterizing the effect of mechanical strain magnitudes on the maturation of iPSC-Cardiomyocytes, *Biosens. Bioelectron.* 175 (2021), 112875, <https://doi.org/10.1016/j.bios.2020.112875>.
 - [33] Y. Liu, N.-E. Oyinbaatar, A. Shanmugasundaram, E.-S. Kim, B.-K. Lee, D.-W. Lee, Nano-textured polydimethylsiloxane cantilever with embedded silver nanowire networks for drug screening applications, *Sens. Actuators B Chem.* 390 (2023), 134014, <https://doi.org/10.1016/j.snb.2023.134014>.
 - [34] J. Kim, A. Shanmugasundaram, D.-W. Lee, Enhancement of cardiac contractility using gold-coated SU-8 cantilevers and their application to drug-induced cardiac toxicity tests, *Analyst* 146 (2022) 6768–6779, <https://doi.org/10.1039/D1AN01337H>.
 - [35] H. Mansour, P.P. de Tombe, A.M. Samarel, B. Russell, Restoration of resting sarcomere length after uniaxial static strain is regulated by protein kinase c ϵ and focal adhesion kinase, *Circ. Res.* 94 (2004) 642–649, <https://doi.org/10.1161/01.RES.0000121101.32286.C8>.
 - [36] K.M. French, J.T. Maxwell, S. Bhutani, S. Ghosh-Choudhary, M.J. Fierro, T. D. Johnson, K.L. Christman, W.R. Taylor, M.E. Davi, Fibronectin and cyclic strain improve cardiac progenitor cell regenerative potential in vitro, *Stem Cell. Int.* 2016 (2016), 8364382, <https://doi.org/10.1155/2016/8364382>.
 - [37] V. Sequeira, L.L. Nijenkamp, J.A. Regan, J. van der Velden, The physiological role of cardiac cytoskeleton and its alterations in heart failure, *Biochim Biophys. Acta Biomembr.* BBA-Biomembranes 1838 (2014) 700–722, <https://doi.org/10.1016/j.bbamem.2013.07.011>.
 - [38] P.P. Kanade, N.-E. Oyinbaatar, A. Shanmugasundaram, Y.-J. Jeong, E.-S. Kim, B.-K. Lee, D.-W. Lee, MEA-integrated cantilever platform for comparison of real-time change in electrophysiology and contractility of cardiomyocytes to drugs, *Biosens. Bioelectron.* 216 (2022), 114675, <https://doi.org/10.1016/j.bios.2022.114675>.
 - [39] C.K. Lam, L. Tian, N. Belbachir, A. Wnorowski, R. Shrestha, N. Ma, T. Kitani, J.-W. Rhee, J.C. Wu, Identifying the transcriptome signatures of calcium channel blockers in human induced pluripotent stem cell-derived cardiomyocytes, *Circ. Res.* 125 (2) (2019) 212–222, <https://doi.org/10.1161/CIRCRESAHA.118.314202>.
 - [40] M.D. Estevez, A. Wolf, U. Schramm, Effect of PSC 833, verapamil and amiodarone on adriamycin toxicity in cultured rat cardiomyocytes, *Toxicol. Vitro.* 14 (2000) 17–23, [https://doi.org/10.1016/S0887-2333\(99\)00087-9](https://doi.org/10.1016/S0887-2333(99)00087-9).
 - [41] L.-R. Jiang, M.-Q. Shen, Y.-X. Bao, Z.-M. Qian, Verapamil downregulates iron uptake and upregulates divalent metal transporter 1 expression in H₉C₂ cardiomyocytes, *Fundam. Clin. Pharm.* 36 (2021) 985–991, <https://doi.org/10.1111/fcp.12793>.
 - [42] D.U. Jeong, K.M. Lim, The effect of myocardial action potential duration on cardiac pumping efficacy: a computational study, *Biomed. Eng. Online* 17 (2018), 79, <https://doi.org/10.1186/s12938-018-0508-2>.
 - [43] R.A. Bouchard, R.B. Clark, W.R. Giles, Effects of Action Potential Duration on Excitation-Contraction Coupling in Rat Ventricular Myocytes, *Circ. Res.* 76 (5) (1995) 790–801, <https://doi.org/10.1161/01.RES.76.5.790>.
 - [44] D.M. Roden, B.F. Hoffman, Action potential prolongation and induction of abnormal automaticity by low quinidine concentrations in canine Purkinje fibers. Relationship to potassium and cycle length, *Circ. Res.* 56 (6) (1985) 857–867, <https://doi.org/10.1161/01.RES.56.6.857>.
 - [45] L. Wu, D. Guo, H. Li, J. Hackett, G.X. Yan, Z. Jiao, C.J.C. Antzelevitch Shryock, L. Belardinelli, Role of late sodium current in modulating the proarrhythmic and antiarrhythmic effects of quinidine, *Heart Rhythm* 5 (2008) 1726–1734, <https://doi.org/10.1016/j.hrthm.2008.09.008>.

Mr. Abdullah Basham received his MS degree in mechanical engineering from Kyungpook National University (KNU), Korea. Currently he is pursuing his doctoral degree in mechanical engineering at MEMS and Nanotechnology Laboratory, Department of Mechanical Engineering, Chonnam National University (CNU), Korea. His research activity is primarily focused on design and fabrication new class of Bio-MEMS device for drug screening applications.

Dr. Arunkumar Shanmugasundaram completed his Ph.D. at the CSIR-Indian Institute of Chemical Technology, Hyderabad, India. Currently he is working as a post-doctoral researcher at MEMS and Nanotechnology laboratory, School of Mechanical Engineering, Chonnam National University (CNU), Korea. His research interests include design and development of next generation sensors for biomedical applications.

Dr. Yun-Jin Jeong obtained his Ph.D. degree in 2018 from department of Mechanical Engineering, Chonnam National University (CNU), Korea. He is currently working as a research professor at MEMS and Nanotechnology Laboratory, Chonnam National University, Korea. His current research interests include Bio-sensors based on MEMS and smart stent

Ms. Pooja P. Kanade is a Ph. D. student in mechanical engineering at the MEMS and Nanotechnology Laboratory, Department of Mechanical Engineering, Chonnam National University (CNU), Korea. She has an interdisciplinary background, with a Bachelors in Electronics engineering and a Masters in Energy systems. Her research activity is focused on the design and development of combined electro-mechanical biosensors and systems for biomedical applications.

Dr. Jongyun Kim obtained his Ph.D. degree in 2021 from department of Mechanical Engineering, Chonnam National University (CNU), Korea. He is currently working as a post-doctoral researcher at MEMS and Nanotechnology Laboratory, Chonnam National University (CNU), Korea. His research activity is primarily focused on developing MEMS-based biosensing platforms for biomedical applications.

Prof. Dong-Weon Lee received his Ph.D. degree in Mechatronics engineering from Tohoku University, Sendai, Japan in 2001. He has been a Professor of Mechanical Systems Engineering at Chonnam National University (CNU), South Korea since 2004. Previously, he was with the IBM Zurich Research Laboratory in Switzerland, working mainly on microcantilever devices for chemical AFM applications. At CNU, his research interests include smart cantilever devices, miniaturized energy harvester, smart structures & materials, and nanoscale transducers. He is a member of the technical program committee of IEEE Sensors Conference, Transducers, and Microprocesses and Nanotechnology Conference.